ACS Catalysis

Letter

pubs.acs.org/acscatalysis

Enhanced Electrocatalytic Activity and Durability of Pt Particles Supported on Ordered Mesoporous Carbon Spheres

Chengwei Zhang,[†] Lianbin Xu,*[,†] Nannan Shan,[†] Tingting Sun,[†] Jianfeng Chen,*[,†] and Yushan Yan[‡]

[†]State Key Laboratory of Organic−Inorganic Composites, Beijing University of Chemical Technology, Beijing 100029, People's Republic of China

[‡]Department of Chemical and Biomolecular Engineering, University of Delaware, Newark, Delaware 19716, United States

Supporting Information

ABSTRACT: Three-dimensionally ordered mesoporous carbon sphere array (OMCS)-supported Pt nanoparticles (Pt/OMCS) were synthesized and studied as electrocatalysts for the methanol oxidation reaction (MOR) and oxygen reduction reaction (ORR). In the Pt/OMCS, the Pt particles with a mean size of ∼1.6 nm are homogeneously dispersed on the mesopore walls of the carbon spheres. The Pt/OMCS catalyst exhibits smaller Pt particle size, greater Pt dispersion, larger specific electrochemically active surface area (ECSA), higher activity for MOR and ORR, and better electrocatalytic stability than the carbon black (Vulcan XC-72R)-supported Pt and commercial Pt/C catalysts.

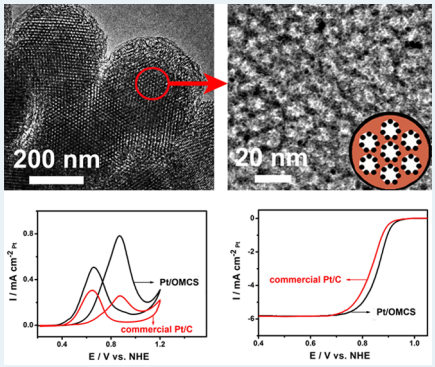

KEYWORDS: *Pt nanoparticles, ordered mesoporous carbon spheres, electrocatalyst, methanol oxidation reaction, oxygen reduction reaction, durability*

As high-efficiency energy conversion and environmentally benign devices, proton-exchange membrane fuel cells (PEMFC) have attracted great attention for transportation and mobile applications.[1,2] The noble metals (such as Pt and Pd) are the most popular and effective catalysts for PEMFC;[3−6] however, the high cost of the noble metals remains one of the biggest hurdles to the commercial applications of PEMFC. Therefore, great efforts have been focused on developing catalysts with high dispersion, proper particle size, and stability to effectively utilize the noble metals and, consequently, lower the cost of PEMFCs. One of the effective ways is developing catalyst supporting materials with large surface areas, high chemical stability, and excellent electrical conductivity. Carbon materials are widely used as catalyst supports that can improve the distribution of noble metal particles and, thus, achieve high utilization of the expensive noble metals.

To further enhance the catalytic activity and durability of the metal/carbon catalysts, there has been in recent years considerable interest in the development of novel nanostructured carbon materials, such as graphene, carbon nanotubes, carbon nanofibers, hollow carbon spheres, and ordered mesoporous carbons as catalyst supports.[7−13] Among them, mesoporous carbon materials as catalyst supports have received growing attention because they can provide a high surface area for highly dispersing catalyst nanoparticles and uniform mesopores for ion diffusion.[8,14] Compared with the generally used bulk mesoporous carbon powders, mesoporous carbon spheres as catalyst supports are more easily accessible for the guest molecules as a result of their high surface-to-volume ratio.[15,16] The organization of monodispersed mesoporous carbon spheres into three-dimensionally (3D) ordered close-packed arrays would offer important advantages for use as catalyst supports in electrocatalysis.

The 3D ordered mesoporous carbon sphere arrays (OMCS) contain hierarchical interconnected macropores (the voids between the close-packed carbon spheres) and mesopores (within individual carbon spheres), which would be desirable to improve the electrocatalytic activity of the catalyst supported on carbon spheres due to the high surface area from the mesopores for high dispersion of the catalyst particles and efficient transport of molecules and ions from the macropores for increasing accessibility to the active sites.[17] In addition, ordered bicontinuous macropores provide a shorter molecule/ion diffusion length in the reaction solution, resulting in more efficient diffusion of reagents compared with the disordered ones.[18,19] The hierarchical combination of ordered macropores and mesopores may allow for extremely fast mass transport within the electrode film. Furthermore, the densely packed carbon spheres would have better electrical conductivity and mechanical properties than the carbon materials with loosely aggregated particles.[20,21]

Received: January 23, 2014
Revised: May 7, 2014
Published: May 8, 2014

   dx.doi.org/10.1021/cs500107t | ACS Catal. 2014, 4, 1926−1930

Generally, materials (e.g., SiO_2,[22] TiO_2,[23] and carbon[20]) with 3D ordered mesoporous sphere array structures can be conveniently prepared by a combination of two-step micromolding (hard templating) and triblock-copolymer-templating (soft templating) approaches. The employment of 3D ordered mesoporous carbon sphere arrays as catalyst supports for the anode and cathode reactions of the PEMFC has not yet been reported. Herein, we first demonstrate the preparation of the Pt nanoparticles supported on 3D ordered mesoporous carbon sphere arrays (Pt/OMCS) and investigate their electrocatalytic properties for the methanol oxidation reaction (MOR) and oxygen reduction reaction (ORR).

The typical preparation of the Pt/OMCS is briefly described by the procedure shown in Scheme 1. The PMMA (poly-

Scheme 1. Schematic of the Synthesis of the Pt/OMCS Catalyst

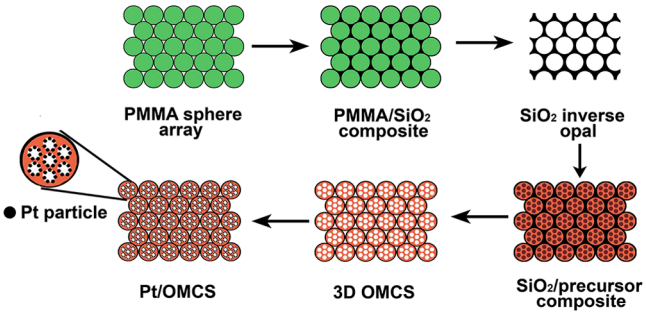

(methyl methacrylate)) colloidal crystals composed of ~460 nm PMMA spheres were first prepared by the published method.[24] Then the PMMA colloidal crystal was used as an initial template to synthesize silica inverse opal. For the production of mesoporous carbon spheres, the silica inverse opal was applied as a further template, the phenolic resol precursor (M_w < 500) was employed as a carbon source, and the triblock copolymer Pluronic F127 acted as a mesopore-structure-directing agent.[20,25] After carbonation and then removal of the silica inverse opal, ordered mesoporous carbon sphere arrays (OMCS) were produced. Finally, the Pt supported on OMCS was prepared by H_2 reduction of Pt ions on the OMCS. The detailed preparation process can be found in the Supporting Information.

Figure 1A shows the typical scanning electron microscopy (SEM) image of the silica inverse opal with uniform macroporous structure. Due to the condensation of silica precursor during calcination,[26] the macropore size shrinks to ~410 nm, ~11% smaller than the diameter of the original PMMA spheres. Figure 1B reveals an SEM image of the ordered mesoporous carbon sphere arrays. Through the two-

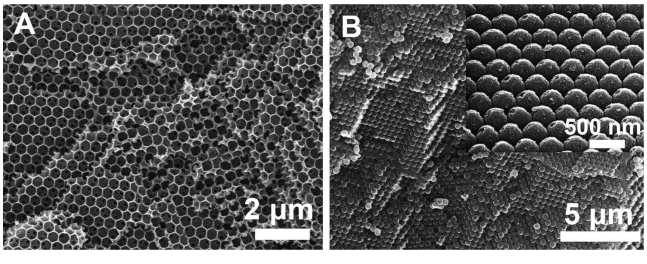

Figure 1. SEM images of (A) the silica inverse opal and (B) OMCS. Inset: OMCS with (111) direction at a higher magnification.

step replication procedure, as-prepared mesoporous carbon still keeps the spherical shape and ordered close-packed face-centered cubic (fcc) structure as in the initial PMMA opal, but the diameter of the carbon spheres is observed to be ~380 nm, ~17% smaller than the original PMMA sphere diameter. This volume contraction is due to the shrinkage of the carbon precursor during the calcination process.[20] Figure 2A shows the

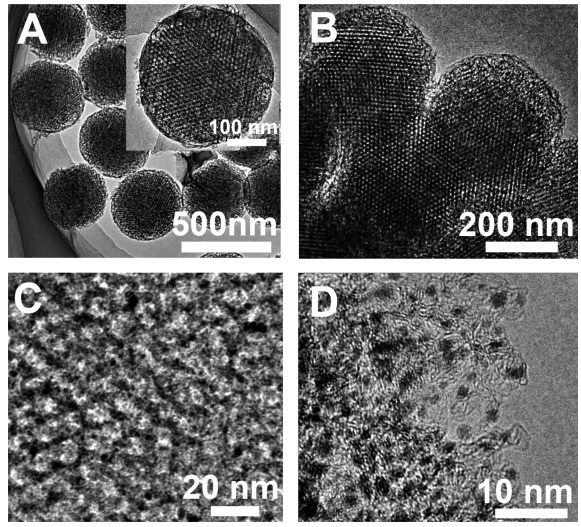

Figure 2. (A) TEM image of the OMCS (inset: higher magnification image of one of the mesoporous carbon spheres), (B) TEM image of the Pt/OMCS, (C) higher magnification TEM image of the Pt/OMCS, and (D) HR-TEM image of the Pt particles on the mesoporous carbon spheres.

transmission electron microscopy (TEM) image of the mesoporous carbon spheres. One of the spheres is enlarged in the inset of Figure 2A and an ordered cubic mesostructure with 7−9 nm cell parameter can be clearly seen. The relatively large mesopore channels of OMCS are beneficial for the growth of Pt nanoparticles on the carbon spheres.

Pt nanoparticles supported on the OMCS (Pt/OMCS) and Vulcan XC-72R (Pt/XC-72R) were prepared for the electrocatalytic reactions. The interconnected network structure with hierarchical macropores and mesopores is well maintained (Figure 2B and Supporting Information Figure S2) after loading Pt particles on the OMCS, which is important for the dispersion of Pt particles and the facile diffusion of reactants during the electrocatalytic electrode reactions.[27,28] Figure 2C is the enlarged TEM image of one carbon sphere and shows that the Pt particles are uniformly dispersed on the mesopore walls of the carbon spheres. From the corresponding high-resolution TEM (HR-TEM) image (Figure 2D), the mean size of the Pt particles on OMCS is about 1.7 nm based on 100 Pt particles randomly selected. The X-ray diffraction (XRD) (Figure 3) was used to further investigate the Pt particle size. The Pt particle sizes of the Pt/OMCS, Pt/XC-72R, and commercial Pt/C (HiSpec3000, Johnson Matthey) catalysts estimated by the Scherrer equation are 1.6, 2.9, and 2.5 nm, respectively, which is in agreement with the HR-TEM observations (Figure 2D and Supporting Information Figure S4). The size of the Pt particles on OMCS is smaller than that on Vulcan XC-72R because of the pore confinement effect that suppresses the growth of Pt particles.[8,28−31]

Figure 4 compares the MOR and ORR performances of the Pt/OMCS, Pt/XC-72R, and commercial Pt/C catalysts. The

dx.doi.org/10.1021/cs500107t | ACS Catal. 2014, 4, 1926−1930

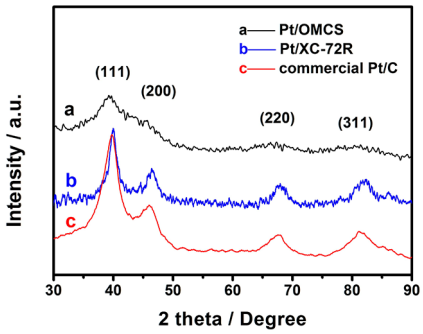

Figure 3. XRD patterns of the Pt/OMCS (a), Pt/XC-72R (b), and commercial Pt/C (c) catalysts.

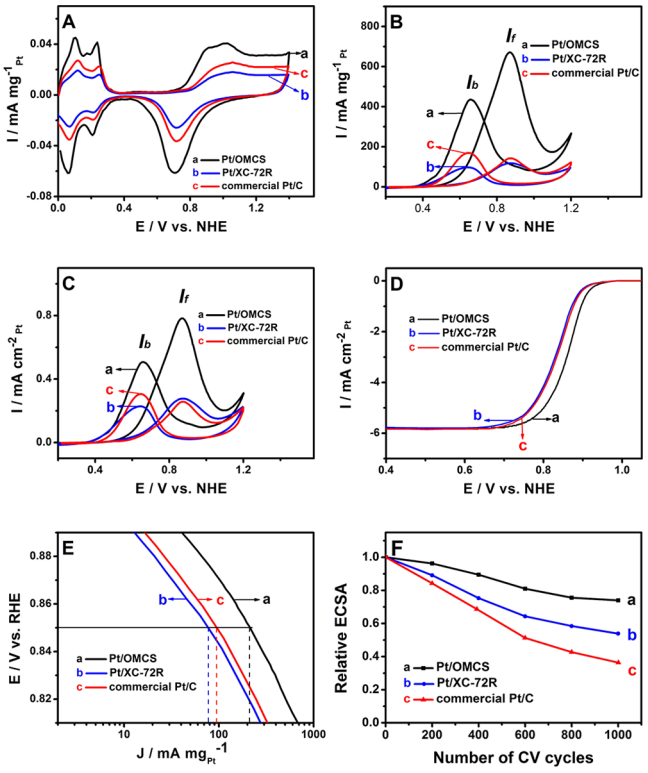

Figure 4. (A) Cyclic voltammograms (CVs) of the Pt/OMCS (a), Pt/XC-72R (b), and commercial Pt/C (c) catalysts in Ar-saturated 0.5 M H_2SO_4; (B) CVs of the catalysts in Ar-saturated 0.5 M H_2SO_4 and 1 M CH_3OH; (C) ECSA-normalized CVs of the catalysts in Ar-saturated 0.5 M H_2SO_4 and 1 M CH_3OH (scan rates for A, B, and C: 50 mV s^{-1}); (D) ORR curves of the catalysts in O_2-saturated 0.5 M H_2SO_4 solution at room temperature (1600 rpm, scan rate: 5 mV s^{-1}); (E) corresponding Tafel plots of the mass activity-potential curve for ORR; and (F) loss of the ECSA of the catalysts with number of CV cycles in Ar-saturated 0.5 M H_2SO_4 solution at room temperature (0–1.3 V vs RHE, scan rate: 50 mV s^{-1}).

electrocatalytic results of the three catalysts are summarized in Table 1. Figure 4A shows the cyclic voltammograms (CVs) in 0.5 M H_2SO_4 solution at a scan rate of 50 mV s^{-1}. The CV curves reveal two distinctive potential regions associated with hydrogen adsorption/desorption (below 0.35 V) and Pt oxidation/reduction (above 0.4 V) processes, respectively.[32−34]

The specific electrochemically active surface area (ECSA) of the Pt/OMCS is calculated to be 85.7 m^2 g^{-1}, which is much higher than that of the Pt/XC-72R (42.5 m^2 g^{-1}) and commercial Pt/C (55.3 m^2 g^{-1}) catalysts. The larger ECSA is ascribed to the smaller and higher dispersion Pt particles of the Pt/OMCS catalyst.[35−37]

The electrocatalytic properties of these catalysts for MOR were tested (Figure 4B and Figure 4C). The Pt/OMCS reaches a forward anodic current peak value of 671 mA mg^{-1}, which is 5.7 times and 4.6 times that of the Pt/XC-72R (118 mA mg^{-1}) and the commercial Pt/C (145 mA mg^{-1}), respectively. After normalization to the ECSA (Figure 4C), the Pt/OMCS exhibits a peak current density of 0.78 mA cm^{-2}, which is still far larger than that of the Pt/XC-72R (0.28 mA cm^{-2}) and the commercial Pt/C (0.26 mA cm^{-2}). In addition, the ratio of I_f (forward anodic current peak) to I_b (reverse anodic current peak) of the Pt/OMCS catalyst is 1.56, which is higher than that of both the Pt/XC-72R (1.21) and the commercial Pt/C (0.86) catalysts. This higher I_f /I_b indicates a better poisoning tolerance of the Pt/OMCS catalyst for MOR.[38] The I_f /I_b value of the Pt/OMCS is comparable to or higher than that of the reported Pt/ordered macroporous carbon spheres (1.60),[39] Pt/mesoporous carbon nanofibers (1.23)[36] and Pt/carbon sphere chains (1.30)[40] catalysts.

The significantly enhanced MOR performance is not fully understood yet, but may be related to the unique hierarchical porous structure of the Pt/OMCS catalyst with highly dispersed Pt particles. The high dispersion of small Pt particles deposited on the mesopore walls of the carbon spheres provides more active sites for the MOR, and the 3D interconnected ordered macropores and mesopores allow the facile transport of the reactant and product molecules and ions to and from the catalyst, increasing the access of methanol to the active sites.[41−44] In addition, owing to the confinement effect of the mesopores of the Pt/OMCS, the methanol molecules are trapped to stay relatively longer and thus be oxidized more efficiently on the surface of the Pt particles.[45,46] The rapid mass transport and more activity sites of the Pt/OMCS may facilitate water dissociation to produce adsorbed OH groups on the catalyst surface that can accelerate the oxidation of the adsorbed CO intermediates, leading to the enhanced poisoning tolerance of the catalyst.[43,47]

Figure 4D shows typical ORR polarization curves of the catalysts obtained in O_2-saturated 0.5 M H_2SO_4 solutions with a scan rate of 5 mV s^{-1} and rotating speed of 1600 r min^{-1} at

Table 1. Pt Mass Contents, Pt Particle Sizes, ECSAs, Peak Current Densities for MOR in the Forward Scan, and ORR Activities at 0.85 V of the Pt/OMCS, Pt/XC-72R, and Commercial Pt/C Catalysts

				peak current density for MOR		ORR activities at 0.85 V	
sample	Pt content[a]	Pt particle size[b] (nm)	ECSA (m^2 g^{-1})	mass activity (mA mg^{-1})	specific activity (mA cm^{-2})	mass activity (mA mg^{-1})	specific activity (mA cm^{-2})
Pt/OMCS	19.4%	1.6	85.7	671	0.78	212	0.25
Pt/XC-72R	19.1%	2.9	42.5	118	0.28	78	0.18
commercial Pt/C	19.6%	2.5	55.3	145	0.26	93	0.17

[a]The data were determined by inductively coupled plasma−atomic emission spectrometry (ICP). [b]The data were calculated by XRD.

dx.doi.org/10.1021/cs500107t | ACS Catal. 2014, 4, 1926−1930

room temperature. The current densities were calculated by normalizing to the geometric electrode area. To compare the catalysts' intrinsic activity, the corresponding Tafel plots are shown in Figure 4E. The kinetic currents of the electrocatalysts are calculated by using the mass-transport correction for rotating disk electrodes:[1]

$$\mathbf{j}_k = \frac{\mathbf{j} \times \mathbf{j}_d}{\mathbf{j}_d - \mathbf{j}} \quad (1)$$

where $\mathbf{j}_k$ is the mass-transport-free kinetic current density, $\mathbf{j}$ refers to the experimentally obtained current density, and $\mathbf{j}_d$ is the measured diffusion-limited current density. The mass activity can be determined by normalizing to the Pt loadings and the specific activity can be determined by normalizing to the ECSAs. The kinetic currents measured from Figure 4E are summarized in Table 1. The kinetic mass current density of the Pt/OMCS at 0.85 V is calculated to be 212 mA mg^{-1}, which is ~2.3 times as high as that of the commercial Pt/C (93 mA mg^{-1}). After normalization to the ECSA, the Pt/OMCS still shows the highest catalytic activity for ORR. The higher ORR activities of the Pt/OMCS catalyst may be attributed to the high dispersion of Pt particles on the mesopore walls of the carbon spheres and the improved mass transfer due to the interconnected macropores between the close-packed spheres and ordered large mesopores.[28,42,48−50]

The durability tests of the catalysts were carried out by cycling the electrode potential between 0 and 1.3 V at a scan rate of 50 mV s^{-1} in argon-purged 0.5 M H_2SO_4 solution at room temperature. As can be seen in Figure 4F, the Pt/OMCS catalyst loses only ~26% of its Pt ECSA after 1000 cycles, whereas that of the Pt/XC-72R and commercial Pt/C catalysts has decreased by 46% and 64%, respectively. The Pt/OMCS, Pt/XC-72R, and Pt/C catalysts were investigated by TEM before and after the durability tests (Supporting Information Figure S4). The increased Pt particle size, the aggregation of Pt particles, and the falling off of Pt particles from the carbon support are considered the major contributors for the Pt ECSA loss of the Pt/XC-72R and commercial Pt/C catalysts. By contrast, there was only slight increase in Pt particle size, but no obvious aggregation of Pt for the Pt/OMCS catalyst after the durability test (Supporting Information Figure S4 and Figure S5). This may be due to the confining effect of the mesopores of OMCS on Pt particles, which further indicates the better stability of the Pt/OMCS catalyst.[34,42,51]

In summary, 3D ordered mesoporous carbon sphere arrays (OMCS) were prepared by a two-step replication approach. The catalyst of Pt nanoparticles supported on OMCS (Pt/OMCS) was successfully fabricated by the hydrogen reduction method. The Pt particles with a mean size of ~1.6 nm are uniformly dispersed on the mesopore walls of the carbon spheres. The Pt/OMCS catalyst exhibits smaller Pt particle size, greater Pt dispersion, higher electrocatalytic performance for MOR and ORR, and better durability than Vulcan XC-72R-supported Pt and commercial Pt/C catalysts. The higher activity of the Pt/OMCS may arise from its unique hierarchical structure with ordered macropores and mesopores that can facilitate the mass transfer and improve the Pt particle dispersion. In addition, the mesoporous structure of the OMCS makes the Pt particles less vulnerable to dissolution and aggregation during the electrocatalytic processes than those supported on the carbon black, leading to a better durability for electrocatalytic reactions. Thus, the Pt/OMCS would be a promising candidate as both the anode and cathode catalysts for the PEMFC.

■ ASSOCIATED CONTENT

Supporting Information

Experimental details and additional information as noted in the text. This material is available free of charge via the Internet at http://pubs.acs.org.

■ AUTHOR INFORMATION

Corresponding Authors

*E-mail: xulb@mail.buct.edu.cn.
*E-mail: chenjf@mail.buct.edu.cn.

Notes

The authors declare no competing financial interest.

■ ACKNOWLEDGMENTS

The authors gratefully acknowledge financial support from the National 973 Program of China (2009CB219903), and the National Natural Science Foundation of China (51172014 and 20971012).

■ REFERENCES

(1) Gasteiger, H. A.; Kocha, S. S.; Sompalli, B.; Wagner, F. T. *Appl. Catal., B* **2005**, *56*, 9−35.
(2) Service, R. F. *Science* **2002**, *296*, 1222−1224.
(3) Huang, S.-Y.; Ganesan, P.; Popov, B. N. *ACS Catal.* **2012**, *2*, 825−831.
(4) Kang, Y.; Murray, C. B. *J. Am. Chem. Soc.* **2010**, *132*, 7568−7569.
(5) Xu, Y.; Hou, S.; Liu, Y.; Zhang, Y.; Wang, H.; Zhang, B. *Chem. Commun.* **2012**, *48*, 2665−2667.
(6) Xu, Y.; Yuan, Y.; Ma, A.; Wu, X.; Liu, Y.; Zhang, B. *ChemPhysChem* **2012**, *13*, 2601−2609.
(7) Wang, C.; Waje, M.; Wang, X.; Tang, J. M.; Haddon, R. C.; Yan, Y. *Nano Lett.* **2004**, *4*, 345−348.
(8) Joo, S. H.; Choi, S. J.; Oh, I.; Kwak, J.; Liu, Z.; Terasaki, O.; Ryoo, R. *Nature* **2001**, *412*, 169−172.
(9) Xia, Y.; Mokaya, R. *Adv. Mater.* **2004**, *16*, 886−891.
(10) Fang, B.; Kim, J. H.; Kim, M.; Yu, J.-S. *Chem. Mater.* **2009**, *21*, 789−796.
(11) Li, W.; Waje, M.; Chen, Z.; Larsen, P.; Yan, Y. *Carbon* **2010**, *48*, 995−1003.
(12) Kou, R.; Shao, Y.; Wang, D.; Engelhard, M. H.; Kwak, J. H.; Wang, J.; Viswanathan, V. V.; Wang, C.; Lin, Y.; Wang, Y. *Electrochem. Commun.* **2009**, *11*, 954−957.
(13) Wen, Z.; Wang, Q.; Zhang, Q.; Li, J. *Electrochem. Commun.* **2007**, *9*, 1867−1872.
(14) Wu, Z.; Lv, Y.; Xia, Y.; Webley, P. A.; Zhao, D. *J. Am. Chem. Soc.* **2012**, *134*, 2236−2245.
(15) Zhang, L.; Kim, J.; Dy, E.; Ban, S.; Tsay, K.-c.; Kawai, H.; Shi, Z.; Zhang, J. *Electrochim. Acta* **2013**, *108*, 480−485.
(16) Barros, F. A. A.; Castro, A. J. R.; Filho, J. M.; Viana, B. C.; Campos, A.; Oliveira, A. C. *J. Nanopart. Res.* **2012**, *14*, 1−12.
(17) Zhang, S.; Chen, L.; Zhou, S.; Zhao, D.; Wu, L. *Chem. Mater.* **2010**, *22*, 3433−3440.
(18) Zhang, H.; Yu, X.; Braun, P. V. *Nat. Nanotechnol.* **2011**, *6*, 277−281.
(19) Huang, H.; Zhang, J.; Zhang, Y.; Lian, S.; Liu, Y. *Solid State Sci.* **2013**, *24*, 115−119.
(20) Liu, H.-J.; Cui, W.-J.; Jin, L.-H.; Wang, C.-X.; Xia, Y.-Y. *J. Mater. Chem.* **2009**, *19*, 3661−3667.
(21) Li, Y.; Fu, Z. Y.; Su, B. L. *Adv. Funct. Mater.* **2012**, *22*, 4634−4667.
(22) Chae, W.-S.; Braun, P. V. *Chem. Mater.* **2007**, *19*, 5593−5597.
(23) Chen, J. F.; Hua, Z. J.; Yan, Y. S.; Zakhidov, A. A.; Baughman, R. H.; Xu, L. B. *Chem. Commun.* **2010**, *46*, 1872−1874.

(24) Schroden, R. C.; Al-Daous, M.; Blanford, C. F.; Stein, A. *Chem. Mater.* **2002**, *14*, 3305−3315.
(25) Meng, Y.; Gu, D.; Zhang, F. Q.; Shi, Y. F.; Yang, H. F.; Li, Z.; Yu, C. Z.; Tu, B.; Zhao, D. Y. *Angew. Chem., Int. Ed.* **2005**, *44*, 7053−7059.
(26) Holland, B. T.; Blanford, C. F.; Do, T.; Stein, A. *Chem. Mater.* **1999**, *11*, 795−805.
(27) Ma, C.; Xue, W.; Li, J.; Xing, W.; Hao, Z. *Green Chem.* **2013**, *15*, 1035−1041.
(28) Joo, S. H.; Pak, C.; You, D. J.; Lee, S. A.; Lee, H. I.; Kim, J. M.; Chang, H.; Seung, D. *Electrochim. Acta* **2006**, *52*, 1618−1626.
(29) Derouane, E. G.; Chang, C. D. *Microporous Mesoporous Mater.* **2000**, *35*, 425−433.
(30) Letellier, F.; Blanchard, J.; Fajerwerg, K.; Louis, C.; Breysse, M.; Guillaume, D.; Uzio, D. *Catal. Lett.* **2006**, *110*, 115−124.
(31) Chang, H.; Joo, S. H.; Pak, C. *J. Mater. Chem.* **2007**, *17*, 3078−3088.
(32) Zhang, C. W.; Yang, H.; Sun, T. T.; Shan, N. N.; Chen, J. F.; Xu, L. B.; Yan, Y. S. *J. Power Sources* **2014**, *245*, 579−582.
(33) Cui, C.-H.; Li, H.-H.; Liu, X.-J.; Gao, M.-R.; Yu, S.-H. *ACS Catal.* **2012**, *2*, 916−924.
(34) Liu, C.; Chen, M.; Du, C.; Zhang, J.; Yin, G.; Shi, P.; Sun, Y. *Int. J. Electrochem. Sci.* **2012**, *7*, 10592−10606.
(35) Chen, Z. W.; Xu, L. B.; Li, W. Z.; Waje, M.; Yan, Y. S. *Nanotechnology* **2006**, *17*, 5254−5259.
(36) Zhao, G. W.; He, J. P.; Zhang, C. X.; Zhou, J. H.; Chen, X.; Wang, T. *J. Phys. Chem. C* **2008**, *112*, 1028−1033.
(37) Zhou, J.-H.; He, J.-P.; Ji, Y.-J.; Dang, W.-J.; Liu, X.-L.; Zhao, G.-W.; Zhang, C.-X.; Zhao, J.-S.; Fu, Q.-B.; Hu, H.-P. *Electrochim. Acta* **2007**, *52*, 4691−4695.
(38) Wang, L.; Yamauchi, Y. *Chem.—Eur. J.* **2011**, *17*, 8810−8815.
(39) Zhang, J.; Zhang, Y.; Lian, S.; Liu, Y.; Kang, Z.; Lee, S.-T. *J. Colloid Interface Sci.* **2011**, *361*, 503−508.
(40) Hamoudi, Z.; El Khakani, M. A.; Mohamedi, M. *Electroanalysis* **2011**, *23*, 1205−1211.
(41) Su, F.; Zeng, J.; Bao, X.; Yu, Y.; Lee, J. Y.; Zhao, X. *Chem. Mater.* **2005**, *17*, 3960−3967.
(42) Yan, Z.; Zhang, M.; Xie, J.; Wang, H.; Wei, W. *J. Power Sources* **2013**, *243*, 48−53.
(43) Zhao, J.; Cheng, F.; Yi, C.; Liang, J.; Tao, Z.; Chen, J. *J. Mater. Chem.* **2009**, *19*, 4108−4116.
(44) Liu, S.-H.; Lu, R.-F.; Huang, S.-J.; Lo, A.-Y.; Chien, S.-H.; Liu, S.-B. *Chem. Commun.* **2006**, 3435−3437.
(45) Bae, J. H.; Han, J.-H.; Chung, T. D. *Phys. Chem. Chem. Phys.* **2012**, *14*, 448−463.
(46) Wang, S.; Kuai, L.; Huang, Y.; Yu, X.; Liu, Y.; Li, W.; Chen, L.; Geng, B. *Chem.—Eur. J.* **2013**, *19*, 240−248.
(47) Wu, J.; Hu, F.; Hu, X.; Wei, Z.; Shen, P. K. *Electrochim. Acta* **2008**, *53*, 8341−8345.
(48) Joo, S. H.; Park, J. Y.; Tsung, C.-K.; Yamada, Y.; Yang, P.; Somorjai, G. A. *Nat. Mater.* **2009**, *8*, 126−131.
(49) Xu, Y.; Zhang, B. *Chem. Soc. Rev.* **2014**, DOI: 10.1039/c3cs60351b.
(50) Yan, Z.; Xie, J.; Zong, S.; Zhang, M.; Sun, Q.; Chen, M. *Electrochim. Acta* **2013**, *109*, 256−261.
(51) Shanahan, P. V.; Xu, L.; Liang, C.; Waje, M.; Dai, S.; Yan, Y. *J. Power Sources* **2008**, *185*, 423−427.